

DEUTSCHES ELEKTRONEN-SYNCHROTRON **DESY**

DESY 87-170
December 1987



HIGH SPEED MONTE CARLO WITH NEUTRON COMPONENT

NEUKA

by

H. Kowalski, H.-J. Moehring, T. Tymieniecka
Deutsches Elektronen-Synchrotron DESY, Hamburg

ISSN 0418-9833

NOTKESTRASSE 85 · 2 HAMBURG 52

DESY behält sich alle Rechte für den Fall der Schutzrechtserteilung und für die wirtschaftliche Verwertung der in diesem Bericht enthaltenen Informationen vor.

DESY reserves all rights for commercial use of information included in this report, especially in case of filing application for or grant of patents.

To be sure that your preprints are promptly included in the
HIGH ENERGY PHYSICS INDEX ,
send them to the following address (if possible by air mail) :

**DESY
Bibliothek
Notkestrasse 85
2 Hamburg 52
Germany**

High Speed Monte Carlo with Neutron Component NEUKA

H. Kowalski, H.-J. Moehring¹, T. Tymieniecka²
Deutsches Elektronen-Synchrotron DESY, Hamburg, FRG

invited talk presented by H. Kowalski
at the Argonne Workshop on Detector Simulation for SSC

to the memory of prof. H. Brueckmann

Introduction

The measurement of energy distributions in hadronic interactions and in particular of jet energies will be one of the most important tasks of the SSC detectors. The precise measurement of jet energies leads to new and stringent requirements on calorimetry which can be only matched by compensating, high resolution calorimeters. The design and construction of such calorimeters requires an extensive test program. Given the size and complexity of hadron calorimeters only a limited number of questions can be studied experimentally and reliable computer calculations, checked against experimental data, are needed for optimizing the calorimeter design.

The compensation effects arise from a "conspiracy" between different energy deposition processes within a hadronic shower. In the hadronic shower there are basically three different energy components:

- Ionization energy deposition from charged hadrons like pions, protons or kaons
- Electromagnetic energy deposition, primarily due to π^0 production, within a shower
- Neutral component from the low-energy nuclear processes, i.e. binding energy losses, emission of evaporation neutrons and heavy fragments.

The relation between the deposited energy and the recorded signal is different for each of the shower components. A realistic MC has to simulate the fluctuations of the shower components in space and from event to event. The fluctuations in hadronic showers are mainly due to high energy hadrons which, in secondary interactions, produce a varying number of other hadrons (e.g. π^- produce many π^0 's or protons produce many neutrons). The shower in which mainly π^0 's were produced has a considerably different shape and correlations than a purely hadronic one. There are also considerable differences between

¹Permanent address: Sektion Physik, Karl-Marx-Universitaet, Leipzig, GDR.

²Permanent address: Institute of Experimental Physics, University of Warsaw, Poland

the hadronic showers containing either predominantly neutrons or charged hadrons. The fluctuations between the charged, electromagnetic and neutral energy components are constrained by the energy conservation requirement. Energy conservation acts in every secondary interaction and leads to complicated energy correlations in space.

π^0 's and evaporation neutrons, once they have been produced, cannot affect the energy sharing between the shower components any more. The photons from π^0 decays shower electromagnetically and have a very low probability of producing any other hadrons. The evaporation neutrons can only reproduce themselves (in fission and nuclear interaction processes).

Existing Monte Carlo programs try to simulate the shower development and the detector response in all details. This requires the simulation of all the events occurring in the shower development down to very low energies of tens of keV for photons, electrons and neutrons. These detailed Monte Carlos are therefore very time consuming and can be applied only to a limited number of calorimeter design questions.

The NEUKA MC, described here, speeds up the simulation by a factor 20 to 40 without affecting significantly the correlations between the fluctuations of the different shower components. This is achieved by:

- the detailed simulation of the hadronic part of the cascade with energy conservation in every secondary interaction - based on the model applied in the FLUKA code, see ref. 1;
- fast parametrization of the most time consuming parts of the shower development, namely the evaporation neutron transport and the electromagnetic energy deposition.

In the following we will describe in some details the models for inelastic secondary interaction (which was directly taken from FLUKA), for evaporation neutron production in uranium and for the interactions of evaporation neutrons with the calorimeter materials. Then we will describe, on the example of the ZEUS uranium scintillator calorimeter, the detection of the neutron, charged and electromagnetic signal. Finally we will discuss the NEUKA results for the calorimeter resolution and e/π ratio and compare them with the experimental tests.

Secondary Interactions

The hadron - nucleus interaction is a superposition of three processes: the nuclear excitation, the intranuclear cascade process and the high energy hadron interaction with the nucleons within the nucleus.

- The nuclear excitation process summarizes the effects of the binding energy losses, neutron evaporation, nucleus excitation and nuclear breakups. These processes are not described in detail. NEUKA determines only (as in FLUKA) the excitation energy, E_{exc} , from a parametrized distribution.

- The cascade protons and neutrons are produced according to the method of Ranft and Routti, ref. 2. The sum of the kinetic energy of all cascade nucleons is equal to the total cascade energy, T_c . T_c is chosen randomly according to an empirically parametrized distribution.
- The hadron interaction with the nucleons are described via resonance production model for projectile energies below 5 GeV. Above 5 GeV the particles are produced via the multi chain exchange model. In both cases the incoming energy is diminished by E_{exc} and T_c to ensure energy conservation.

Evaporation Neutron Production

Evaporation neutrons are produced in every secondary interaction. To determine their number and energy distributions we used the following simple model.

We define first the fraction of excitation energy which is evaporated by neutrons, f_{exc} . The energy necessary to evaporate a neutron is the sum of its kinetic energy and the binding energy within the nucleus. The mean number of evaporated neutrons is therefore given by

$$\bar{n}_{evap} = \frac{f_{exc} \cdot E_{exc}}{\bar{E}_B + \bar{E}_{n,ev}}$$

where

- \bar{E}_B denotes the average neutron binding energy. We assumed $\bar{E}_B = 6.4$ MeV, which is equal to the binding energy of outer shell neutrons in uranium.
- $\bar{E}_{n,ev}$ denotes the average neutron kinetic energy. This energy is expected to be between 3 and 4 MeV. We assumed $\bar{E}_{n,ev} = 3.5$ MeV.

In every secondary interaction the number of neutrons is chosen randomly from a Poisson distribution with the average \bar{n}_{evap} . We note, that this can lead to a small violation of the energy conservation. The neutron kinetic energy is randomly chosen according to the distribution

$$f(E_{n,ev}) = E_{n,ev} \cdot \exp(-2 \cdot E_{n,ev}/\bar{E}_{n,ev})$$

The value of the parameter f_{exc} was determined from the comparison of NEUKA results with the number of captured neutrons, measured from a 591 MeV proton beam incident on U/Sci calorimeter, ref. 3. The measured number of captured neutrons was 21 ± 3 per event. The number of evaporation neutron differs from the number of captured neutrons since an evaporation neutron can produce additional neutrons through fissions or (n,2n) processes. The ratio between the two numbers was determined in several independent calculations, e.g. ref. 4, to be 1.4. In Fig. 1 we show the number of neutrons as a function of f_{exc} determined in the NEUKA simulation of 591 MeV proton interactions. From this figure we determine that $f_{exc} = 0.6 \pm 0.1$.

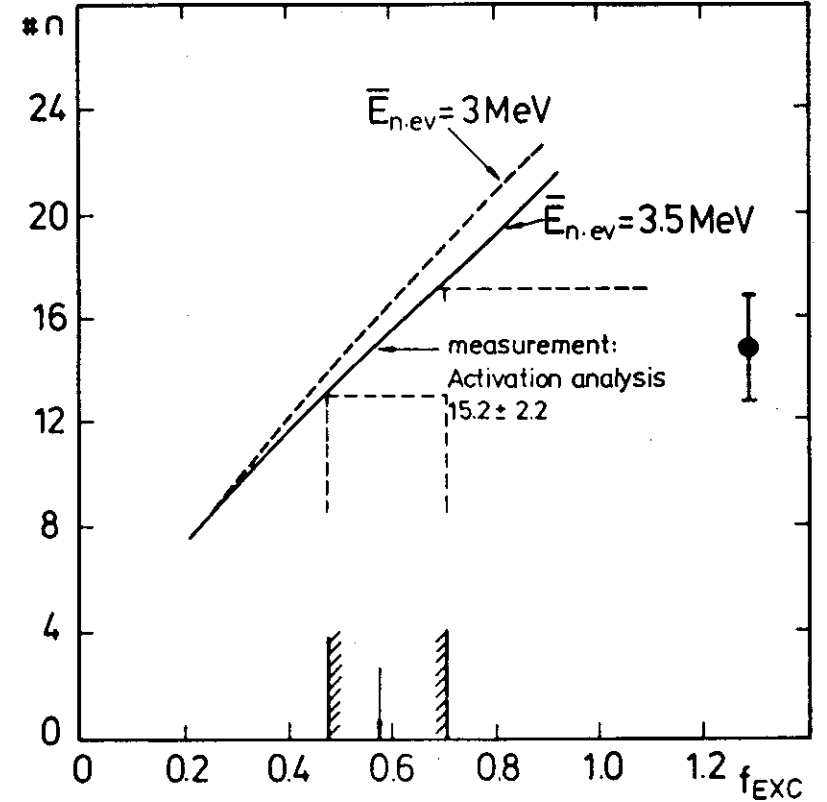


Fig. 1. Number of evaporation neutrons per event as a function of f_{exc} . NEUKA simulation of a 591 MeV proton beam incident on U/Sci calorimeter of ref. 3.

Having determined f_{exc} from the data we have predicted the number of neutrons produced by a π^- beam in the ZEUS calorimeter. The results are given in Table 1.

Table 1. Predicted number of neutrons per incoming π^- , $E_n \leq 20\text{MeV}$

Beam Energy (GeV)	number of neutrons	number of sec.interactions
5	190	7.4
10	320	17
20	610	31
50	1330	60
100	2440	110
200	4370	190
1000	18100	900

In order to avoid the leakage problem we assumed in this calculation that the calorimeter has an infinite size. The thickness of uranium and scintillator plates was taken to be 0.33 and 0.26 cm. We counted all neutrons with $E_n \leq 20\text{ MeV}$.

We observe that the number of produced neutrons per incoming particle and per GeV decreases with the increasing beam energy. This is due to the increase of the electromagnetic component in the shower with the projectile energy.

We remark that in NEUKA MC the low energy neutrons are produced not only from the excitation energy but also from the high energy induced fission (60% probability per secondary interaction) and cascade processes. Let us denote by E_{neu} the sum of kinetic energies (below 20 MeV) of all neutrons produced in an hadronic shower. Then, typically, 60% of E_{neu} is due to evaporation, 20% to fission and 20% to cascade neutrons (for $f_{exc} = 0.6$). In the above numbers we do not count the neutrons produced in the neutron induced low energy fission and interaction processes ($E_n \leq 20\text{MeV}$). The effects of these neutrons are taken into account in the determination of the calorimeter response to the evaporation neutrons as discussed in the next section.

In our model E_{neu} is on the average proportional to f_{exc} , but it fluctuates from event to event. We investigated this fluctuation in the following way. First we determined, for a given f_{exc} , the ratio

$$\alpha = \overline{E}_{neu} / \overline{E}_{exc}$$

E_{exc} denotes here the sum of all excitation energies in an event and the average is taken over all events. Then the variable ξ was defined as

$$\xi = \frac{E_{exc} - E_{neu}/\alpha}{\sqrt{E_{exc}}}$$

The mean square fluctuation of E_{neu} around $\alpha \cdot E_{exc}$ is then

$$\sigma_{exc}^2 = \int \xi^2 f(\xi) d\xi$$

where $f(\xi)$ denotes the distribution of the variable ξ determined from all events.

In Table 2 we give, for a 10 GeV π^- shower, the dependence of E_{neu} and σ_{exc} from f_{exc} as determined in NEUKA.

Table 2. E_{neu} and σ_{exc} as a function of f_{exc}

f_{exc}	0.2	0.4	0.6	0.8	1.0
E_{neu} in % of E_{exc}	20.0	27.3	35.3	42.5	50.5
$\sigma_{exc}/\sqrt{E_{exc}}$ in %	35.0	29.0	23.6	20.9	18.7

The relation between E_{exc} and the energy of the emitted neutrons is independent of projectile energy. The amount of excitation energy, E_{exc} , decreases with increasing beam energy, see Table 3.

One - Neutron Monte Carlo

To understand the mechanism of neutron energy deposition it is necessary to follow the neutrons one by one on their way through the calorimeter. Therefore, we developed a special Monte Carlo to simulate the behaviour of neutrons in the calorimeter.

A low energy evaporation neutron undergoes several reactions: elastic, fission inelastic, (n,2n), (n,3n) and capture interactions with U^{238} and elastic interactions with carbon and hydrogen. The total cross - section for these interactions are given in Fig. 2. To get a feeling for the spatial distributions of the neutrons we remark that for 2 MeV neutrons a mean free path for elastic interaction in pure uranium is 4.7 cm. For inelastic reactions it is 7.8 cm and for fission 38 cm. In the following we describe these interactions in some detail:

- neutron elastic scattering on U. A neutron loses only a small part of its energy (1/239) per collision. The angular distribution is of the coherent elastic type, ref. 2.
- neutron fission of U. In the neutron fission process there are on average 2.5 neutrons produced. The energy of fission neutrons was chosen according to a Maxwell distribution of temperature $\sim 1.33\text{ MeV}$. The number of fission neutrons and their temperature was assumed to depend slightly on the incoming neutron energy in accordance with ref. 6. The fission neutrons were emitted with an isotropic distribution in the laboratory frame.
- neutron inelastic scattering on U. To describe the amount of energy lost by a neutron in this process we used for the low energy neutrons ($\leq 2.5\text{ MeV}$) the nuclear level excitation model by Sheldon, ref. 7. In this model the neutron excites one of the uranium levels and loses the corresponding level energy. The average energy loss by

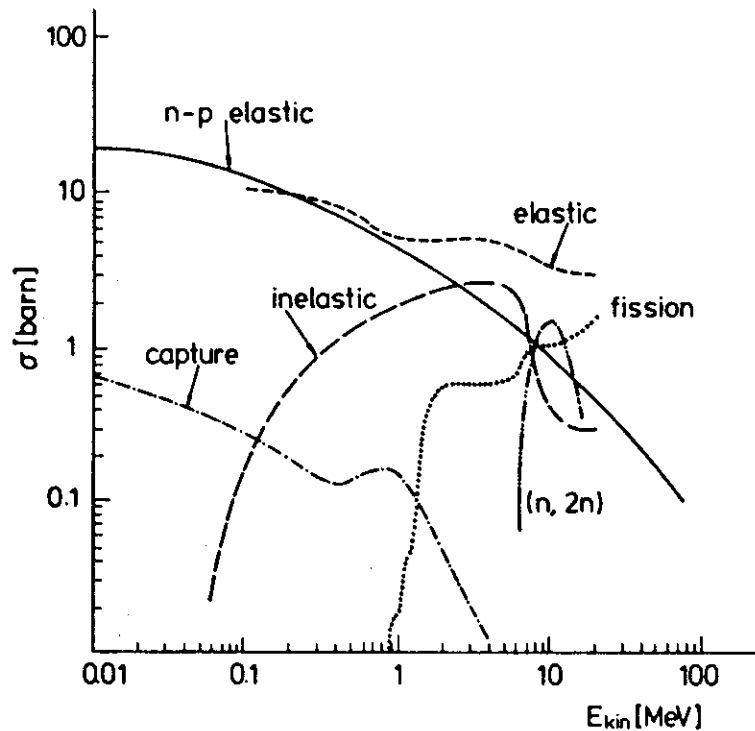


Fig. 2. Cross sections for neutron - U^{238} and neutron - proton interactions as a function of the neutron kinetic energy

a 2 MeV neutron is around 550 KeV. In the higher energy region, above 6 MeV, we used the statistical model of the excited nucleus, ref. 8. In this model, it is assumed that the neutron merges with the nucleus and forms a compound nucleus which then evaporates one, two, or three neutrons. The number of evaporated neutrons is determined by the inelastic, $(n,2n)$ and $(n,3n)$ cross section of Fig. 2. For the evaporation energies we used the phenomenological distributions given in ref. 9. They correspond to a Maxwell spectrum with temperatures between 0.3 and 0.6 MeV for neutron energies between 3 and 6 MeV.

In the region between 2.5 and 6 MeV we assumed that inelastic scattering occurs as a mixture of the above two models. This mixture is determined in the following way: we attach to each model a probability that the inelastic scattering happens according to this model; at 2.5 (6.0) MeV the probability for occurring of the level excitation process is 1 (0) and of the statistical process is 0 (1); in between 2.5 and 6 MeV these probabilities vary linearly with energy.

In the inelastic process a neutron loses a substantial part of its energy and, with a high probability, falls below the fission threshold. Since the inelastic cross section is considerably bigger than the fission one, the inelastic process prevents the neutron proliferation in the uranium calorimeters.

- neutron capture in U. In this process an excited U^{239} nucleus is formed which subsequently decays with the emission of a 4.8 MeV photon to U^{239} . These photons are not simulated in NEUKA. This process is very important for neutron energies below 10 keV.
- neutron elastic scattering on H. In this process the neutron loses on average half of its kinetic energy. In scintillator material the recoil protons produce an ionization signal.
- neutron scattering on C. To describe the n-C interactions we considered the elastic, inelastic and absorption process. In inelastic scattering only the excitation of the 4.3 MeV level was considered.

With the help of the One - Neutron MC we predicted the space distributions of captured neutrons and fission products observed in the activation analysis measurement of ref. 3. In Fig. 3 we show the comparison with data of the transverse distributions for captured neutron and fission products. In Fig. 4 we show the comparison for the longitudinal distribution of fission products. In both cases good agreement is observed.

Detection of Neutron Signal

In our investigation of neutron effects in uranium calorimeters we simulated the neutron source with a Maxwell energy distribution of temperature 2.4 MeV. The energy distribution

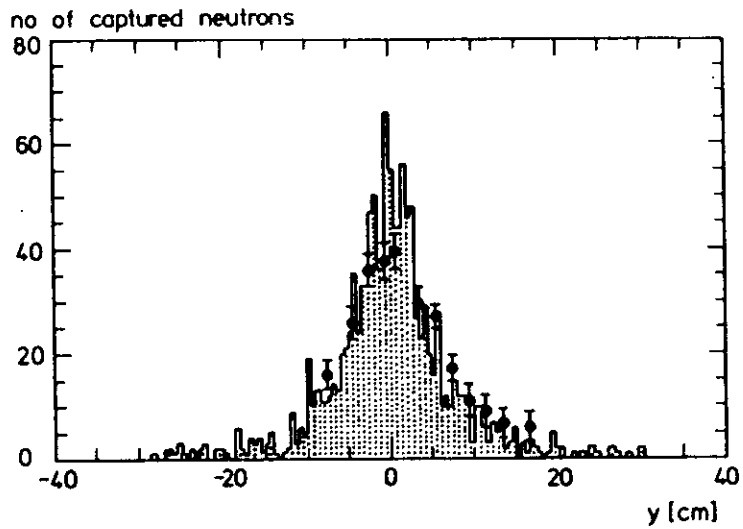


Fig. 3a. Transverse distribution of captured neutrons computed in the O-N MC and compared to the activation analysis results of ref. 3.

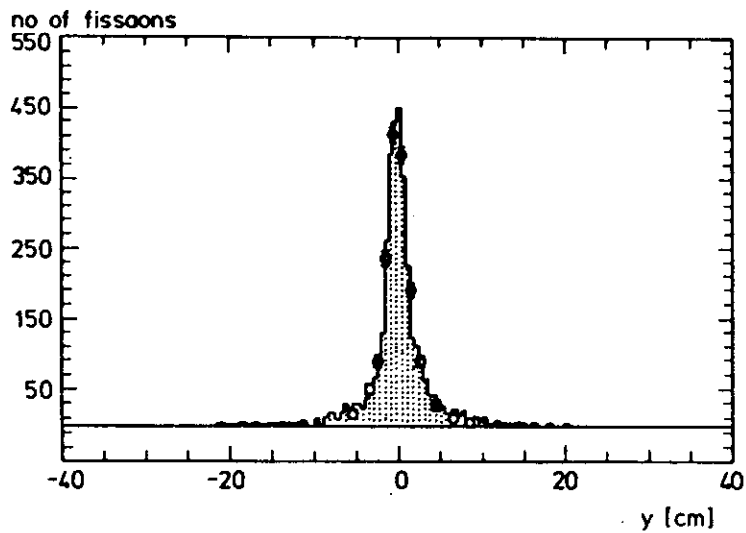


Fig. 3b. Transverse distribution of fissions computed in the O-N MC and compared to the activation analysis results of ref. 3.

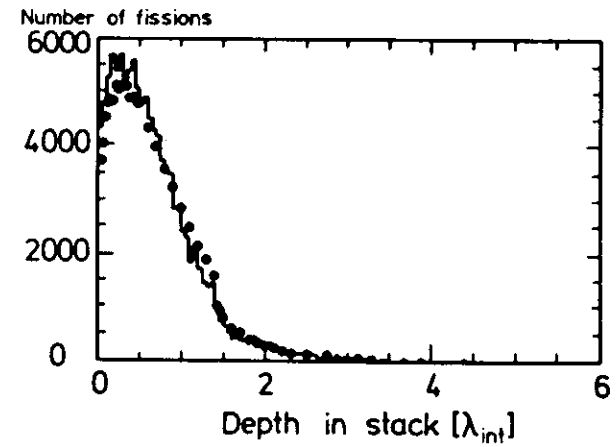


Fig. 4. Logitudinal distribution of fissions computed in the O-N MC and compared to the activation analysis results of ref. 3.

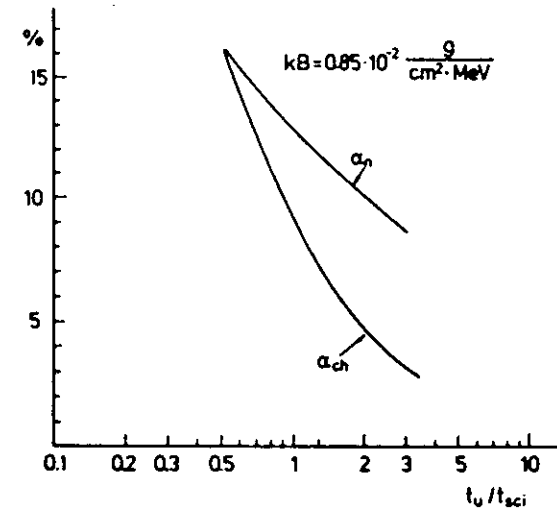


Fig. 5. α_n and α_{ch} as a function of the uranium to scintillator thickness ratio.

was corrected in the low and high energy regions ($E_n \leq 0.5$ and $E_n \geq 15$ MeV) to agree with the experimental observations of ref. 10. The evaporation neutrons transfer their energy to uranium, mainly through the inelastic scattering processes, and to scintillator, through the elastic scattering on hydrogen protons. The amount of energy deposited in uranium and scintillator depends on their relative abundance in the calorimeter measured e.g. by the ratio of the plate thickness. In the uranium scintillator calorimeter with the ZEUS structure $\sim 50\%$ of the energy is deposited in uranium and $\sim 50\%$ in scintillator.

An evaporation neutron travelling through the ZEUS calorimeter produces in the scintillator, on the average, 10 recoil protons with the average energy of 0.2 MeV. The energy of the recoil protons is only partially recorded because the light saturation effects damps the signal. To describe these effects we used the Birks formulae

$$L = \int \frac{dE/dx}{1 + k_b \cdot dE/dx} dx$$

with the $k_b = 0.0085 \text{ g/MeV} \cdot \text{cm}^2$. After the light saturation effects are taken into account only $\sim 20\%$ of recoil proton energy is turned into light. The efficiency of the neutron signal collection is called the sampling fraction for neutrons, α_n , and is defined as a fraction of the kinetic energy of the emitted neutron transferred to the signal taking into account the light saturation effects. An emitted neutron may produce other neutrons through fission or $(n,2n)$ reactions. This effect is automatically included in the α_n determination because, in the O-N MC, the signal is collected from all recoil protons, irrespective of their origin. In Fig.5 we show the sampling fractions for neutrons as a function of the uranium to scintillator plate thickness. For the ZEUS calorimeter we see that the neutron sampling fraction is around 10%.

The O-N MC can also determine the precision of neutron signal detection, σ_{neu} . We found for ZEUS calorimeter that $\sigma_{neu} \sim 9\% \cdot \sqrt{E_{neu}}$. The good resolution for the neutron signal detection is due to the fact that neutrons, other than e.g. charged particles, deposit a large fraction of their energy in the scintillator.

The neutron signal is deposited by several recoil protons. The mean free path of the neutron between subsequent hydrogen elastic scattering varies strongly with neutron energy, see Fig. 2 and is of the order of few centimeters. This leads to a space distribution of the neutron signal. In Fig. 6 we show the transverse distribution for the ZEUS calorimeter as a function of the distance to the point of neutron emission.

In the evaluation of the neutron signal in the hadronic shower it is difficult to follow all the neutrons because the O-N MC is time consuming (20 neutrons/sec of IBM 3084). To evaluate the neutron signal we have therefore used the following recipe:

- subdivide the energy of each individual neutron into n equal "pieces". n is a free parameter with default value $n = 10$.

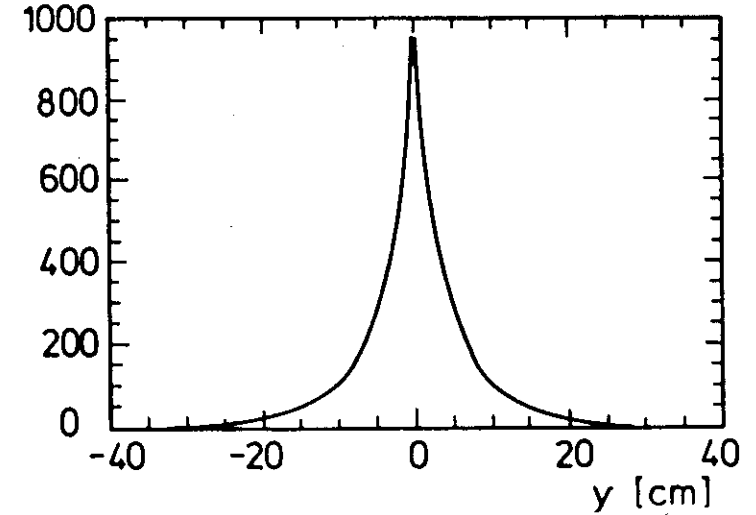


Fig. 6. Space distribution of the neutron signal determined in O-N MC

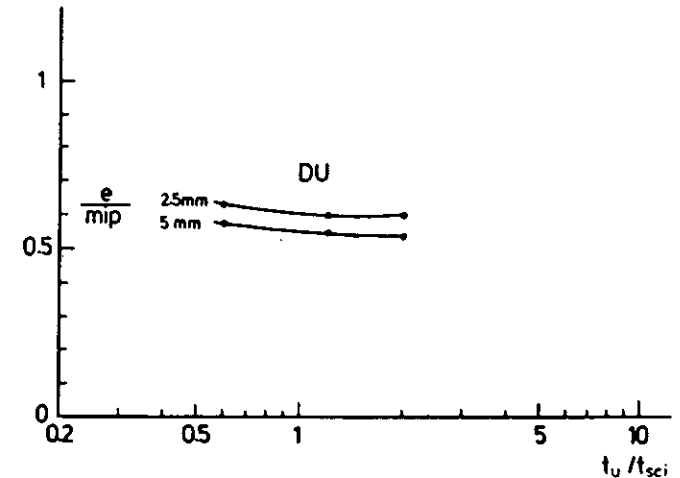


Fig. 7. e/mip ratio as a function of the uranium to scintillator thickness ratio, ref. 4.

- deposit the energy "pieces" at discrete space points, randomly chosen with the space distribution of Fig. 6
- sum up all the energy "pieces" in the calorimeter region of interest. We denote this sum by E_{neu}
- "smear" E_{neu} in a gaussian way with σ_{neu} . The smeared energy is called E_{neu}^{sm} .
- assume that neutron signal = $\alpha_n \cdot E_{neu}^{sm}$

It is interesting to observe that in the hadronic shower only a small part of the excitation energy, E_{exc} , is turned into signal. From the values of E_{neu} given in Table 2 and from the value of $\alpha_n \approx 10\%$ we find that only $\sim 3.5\%$ of E_{exc} is recorded as a signal.

Detection of Charged and Electromagnetic Signal

In this section we discuss the signal due to the charged hadrons and π^0 's directly produced in the secondary interactions of hadronic shower particles. We do not consider here the neutron recoil proton signal which was discussed in the previous section because, in our subdivision of shower energy types, it belongs to the excitation energy component.

Charged hadrons like pions or protons are tracked through the detector taking into account the ionization energy losses. We use the ionization energy loss formula of Bichsel, ref. 1, as in FLUKA program. In our calculation the cut-off for hadron energies was 1 MeV (it was 1 keV for the recoil protons produced by evaporation neutrons in the scintillator). The signal due to charged hadrons was computed in the conventional way by summing up the ionization energy deposited in the scintillator. We denote this signal by E_{ion}^{sci} . We determined also E_{ion}^{tot} which is equal to the ionization energy deposited in the uranium and scintillator. The charged sampling fraction is then

$$\alpha_{ch} = \overline{E_{ion}^{sci}} / \overline{E_{ion}^{tot}}$$

The charged sampling fraction was found to be independent of projectile energy and equal to $\sim 7.5\%$. The charged deposition has two fairly independent components: the charged pions, $E_{ion}^{\pi^\pm}$, and the proton energy deposition, E_{ion}^p . The charged pions are relatively energetic and behave more like minimum ionizing particles. The protons are mainly produced in the intranuclear cascade processes. They are less energetic and therefore can be stopped even in a single absorber plate. In Table 3 we give an overview of the amount of charged pions and proton energy deposition within a hadronic shower. The energy deposition of other charged hadrons can be neglected. α_{ch} was determined to be around 7.3% for pions and around 7.6% for protons.

In Table 3 we give an overview of the amount of charged pions and proton energy deposition within a hadronic shower. The energy deposition of other charged hadrons can

be neglected. The charged energy is compared with the electromagnetic energy deposition, E_{ele} , and to the excitation energy.

Table 3. E_{exc} , $E_{ion}^{\pi^\pm}$, E_{ion}^p and E_{ele} as a function of π^- beam energy

E_{beam} GeV	5	10	20	100	200	1000
E_{exc} GeV	2.02	3.21	6.3	25.5	45.6	188
% of E_{beam}	40.4	32.1	31.5	25.5	22.8	18.8
$E_{ion}^{\pi^\pm}$ GeV	0.75	1.31	2.1	8.0	14.8	61
% of E_{beam}	15.1	13.1	10.6	8.0	7.4	6.1
E_{ion}^p GeV	0.41	1.16	2.2	8.12	14.8	61
% of E_{beam}	8.2	11.6	11.2	8.12	7.4	6.1
E_{ele} GeV	1.35	3.1	7.2	49.8	110	630
% of E_{beam}	27.2	31.3	35.5	49.8	55	63.0

The electromagnetic energy deposition is simulated with the help of a simple parametrization, see ref. 1. This parametrization is similar to the one we used for the evaluation of the neutron signal. The shape of the electromagnetic cascade was determined with the EGS program and data, ref. 11.

The radial distribution of the energy of an individual γ or electron is given by

$$f(r) = 1.1 \cdot \exp(-2.28 \cdot r) + \exp(-0.635 \cdot r)$$

where r is expressed in Moliere units.

The longitudinal shower development is parametrized as

$$f(z) = z^a \cdot \exp(-b \cdot z)$$

where $a = 2.0 - Z/340 + (0.664 - Z/340) \cdot \ln(E)$ and $b = 0.634 - 0.0021 \cdot Z$. Z is the atomic number of the material, E is a photon or electron energy in GeV and z is expressed in radiation lengths.

For every energy "piece" of the electromagnetic cascade, r and z are chosen according to the above distributions. The position of the space points is computed from r and z taking into account the radiation lengths and atomic numbers of different materials in the calorimeter.

To obtain the calorimeter signal we first summed up all the energy "pieces" in the considered calorimeter region, E_{ele} . To simulate the calorimeter measurement effects E_{ele} was "smeared" with the electromagnetic resolution, σ_{ele} which is well known from experiments and EGS calculations. For the ZEUS calorimeter structure it is $\sigma_{ele} = 15\% \cdot \sqrt{E_{ele}}$ and it scales as $\sqrt{t_{abs}}$, where t_{abs} denotes the absorber plate thickness. The smeared electromagnetic energy was denoted as E_{ele}^{sm} .

To compute the signal of the electromagnetic component E_{ele}^{sm} was multiplied by the charged sampling fraction, α_{ch} , and the e/mip ratio to take into account transition effects. The e/mip ratio was determined for different calorimeter structures in ref. 4. The results are shown in Fig. 7.

The resolution for detection of the charged hadron signal, σ_{ch} , can be only investigated with the help of a MC because in nature the charged signal is always mixed with the other shower components. In NEUKA we evaluated the charged resolution, σ_{ch} , in a similar way to σ_{exc} , from the distribution of the variable ξ

$$\xi = \frac{E_{ion}^{tot} - E_{ion}^{exc} / \alpha_{ch}}{\sqrt{E_{ion}^{tot}}}$$

We found that the charged resolution in hadronic showers is very similar to the electromagnetic resolution, $\sigma_{ch} = 15\% \cdot \sqrt{E_{ion}^{tot}}$. This is, however, a coincidence, because the resolution is very different for charged pions, $\sigma_{ch}^{\pi^{\pm}} = 9\% \cdot \sqrt{E_{ion}^{\pi^{\pm}}}$, and protons, $\sigma_{ch}^p = 27\% \cdot \sqrt{E_{ion}^p}$. The poor proton resolution is due to the fact that most protons result from the intranuclear cascade processes. They have therefore lower energies and can be stopped in a single uranium plate.

Calorimeter Resolution and e/π ratio

We investigated the calorimeter resolution and e/π ratio simulating the hadronic shower development in an infinitely large calorimeter with the ZEUS layer structure. The signal was evaluated separately for every shower component, as we discussed above, and then added together,

$$\text{signal} = \alpha_n \cdot E_{neu}^{sm} + E_{ion}^{sci} + e/mip \cdot \alpha_{ch} \cdot E_{ele}^{sm}$$

The measurement precision of the signal, σ/\sqrt{E} and the e/π ratio are shown as a function of beam energy, E , in Fig. 8. We see that σ/\sqrt{E} is almost independent of beam energy and around 30%. e/π is 1.04 for lower energies and it approaches 1.0 as the energy increases due to the increase of the electromagnetic shower component.

To demonstrate the difference between U/Sci and conventional calorimeters we show in Fig. 9 σ/\sqrt{E} computed without the excitation energy contribution. We see that the lack of signal from the excitation energy deteriorates the hadronic resolution at 10 GeV from 30% to 60%. Furthermore the resolution is strongly energy dependent, it increases to 95% at 100 GeV.

The resolution of U/Sci calorimeters for measuring hadronic showers is considerably better than that of conventional calorimeters but, on the other hand, it is worse than the resolution for measuring electromagnetic showers. There are mainly two effects which deteriorate the resolution of U/Sci calorimeters:

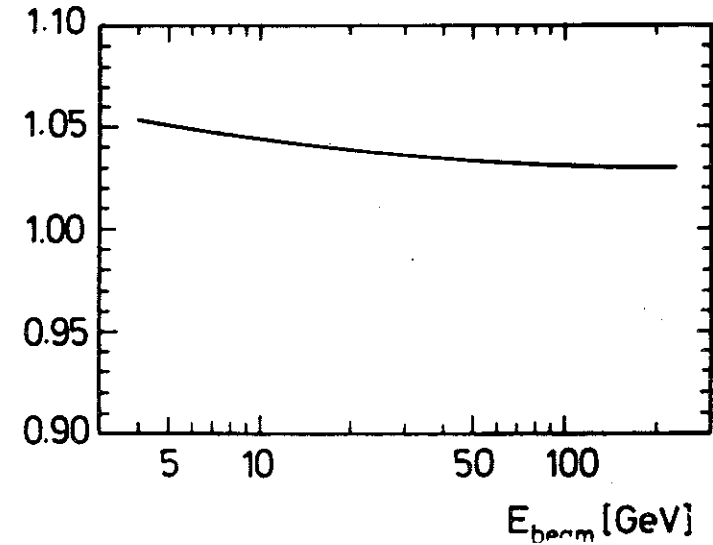
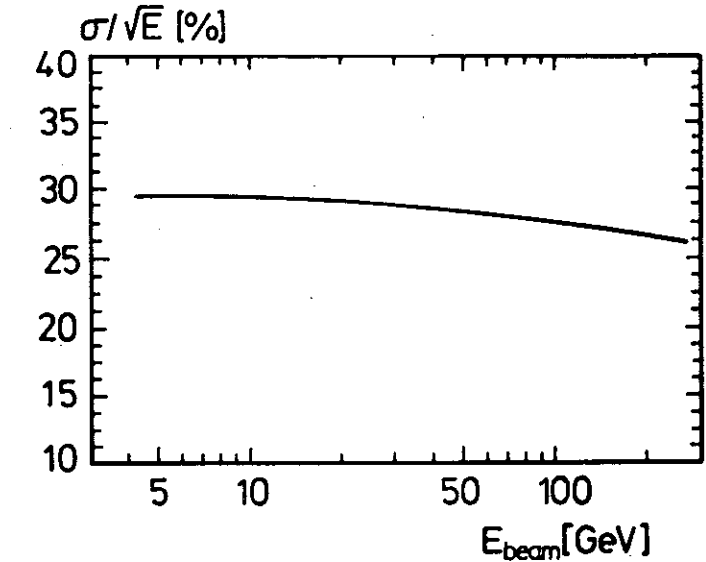


Fig. 8. Resolution and e/π ratio as a function of the beam energy. NEUKA simulation of a π^- beam incident on the infinite calorimeter with ZEUS structure.

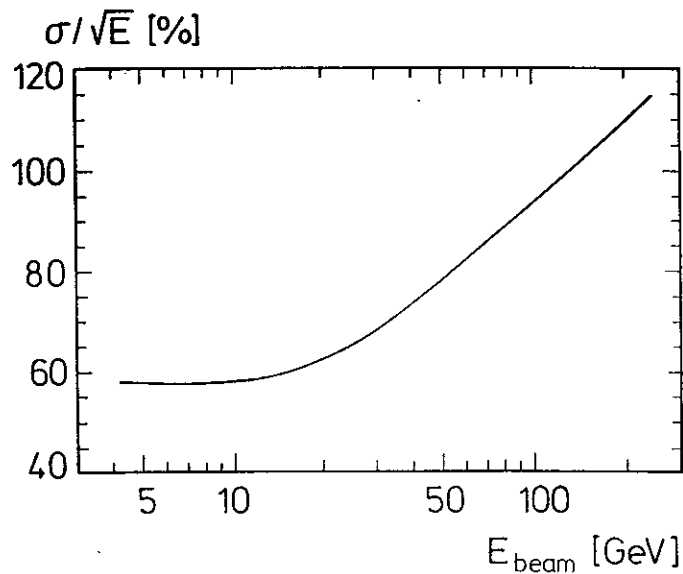


Fig. 9. Resolution as a function of the beam energy evaluated without the neutron contribution. NEUKA simulation of a π^- beam incident on the infinite calorimeter with ZEUS structure.

- the efficiencies for recording different shower components are not completely equal; the excitation energy is recorded with $\sim 3.5\%$, the charged pion energy with 7.3% , the proton energy with $\sim 7.6\%$ and the electromagnetic energy with $\sim 4.5\%$ efficiency.
- the measurement precision of excitation energy is, in our model, fairly poor because of fluctuations of evaporation neutron number and energies, $\sigma_{exc} \oplus \sigma_{neu} = 25\% \cdot \sqrt{E_{exc}}$

The third effect which could affect the resolution is the poor measurement precision of the proton signal ($27\% \cdot \sqrt{E_{ion}^p}$) which is due to stopping of low energy protons in absorber plates. This effect would play an important role in the case that we underestimate considerably the amount of shower energy deposited through protons.

The experimenter can, to some extent, influence the mismatch of different shower component measurement efficiencies. This can be done by varying the thickness of absorber or scintillator plates or adding other materials to the calorimeter. Therefore it is interesting to investigate how the calorimeter resolution varies as a function of different sampling fractions. In Fig. 10 we show the calorimeter resolution as a function of the neutron sampling fraction, α_n . We see that with $\alpha_n \sim 10\%$ ZEUS calorimeter is at the optimum position of the resolution curve. However, reduction of α_n (e.g. due to neutron energy losses) should be avoided because the resolution may rapidly deteriorate.

In Fig. 11 we show NEUKA predictions for the dependence of the resolution on the ratio of uranium to scintillator plate thickness. We see that NEUKA predicts a relatively flat minimum in contrast to the predictions of e.g. ref. 5. If correct it means that it is possible to increase the uranium plate thickness without considerably affecting the hadronic resolution.

Comparison with Test Results

With the help of NEUKA we have studied the energy resolution and transverse energy distribution observed in Test 35. In Fig. 12 we show the simulated energy deposition of a 5 GeV π^- beam. The resolution determined with 2σ gaussian fits is $\sigma/\sqrt{E} = 33.3\%$ which is in good agreement with observed resolution of 33 to 34%. It is interesting to observe that the resolution determined for Test 35 differs from the resolution of 30% expected for infinite calorimeter. The difference is due to energy leakage through the front, sides and back walls which accounts for ca. 10% of the deposited shower energy.

In Fig. 13 we show the comparison of longitudinal shower development profiles observed in test WA78 and the NEUKA predictions for 20 and 40 GeV beam energies. We see that the predictions with neutron energy deposition agree well with data. In Fig. 14 we show a more detailed comparison of energy distributions in the first six modules of test WA78 with NEUKA predictions.

We have also studied, with NEUKA, the effects of introducing a steel plate into the calorimeter structure after one interaction length. In Fig. 15 we show the resolution for

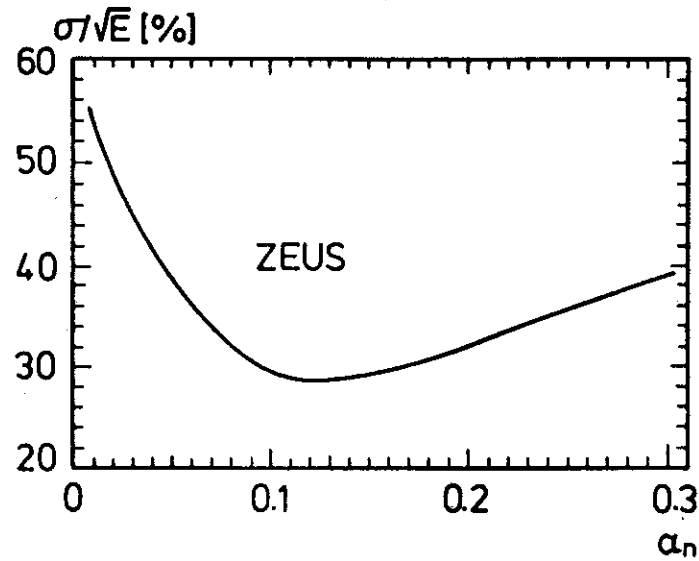


Fig. 10. Calorimeter resolution and e/π ratio as a function of the neutron sampling fraction, α_n . NEUKA simulation of a 10 GeV π^- beam incident on the infinite calorimeter with ZEUS structure.

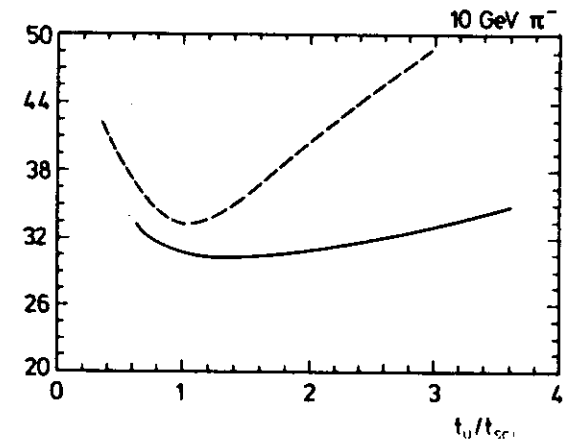
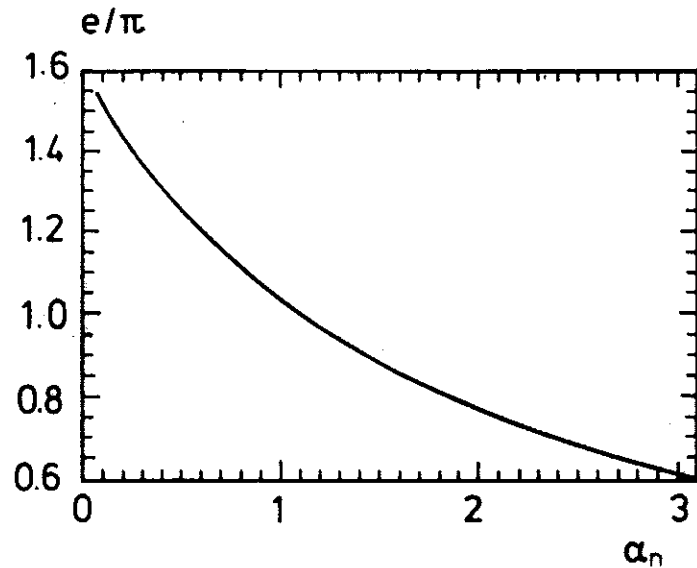


Fig. 11. Calorimeter resolution as a function of the uranium to scintillator thickness ratio. The full line shows the NEUKA simulation and the dashed line the prediction of ref. 5. for a 10 GeV hadron beam.

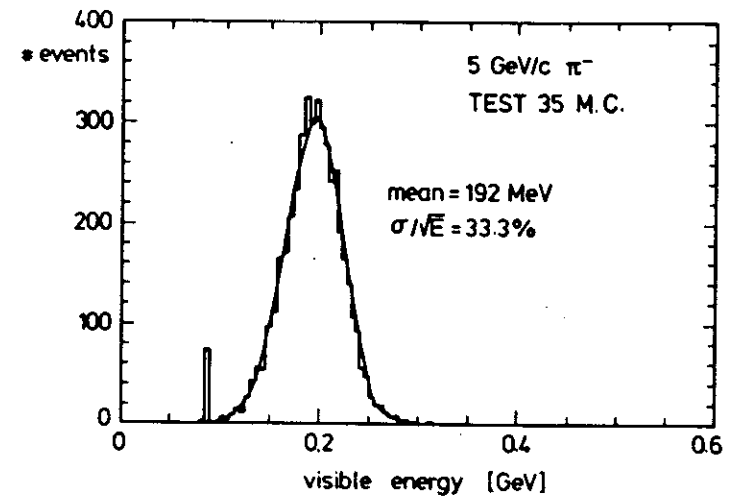


Fig. 12. NEUKA prediction for the response of 5 GeV π^- in Test 35. The resolution is determined with 2σ gaussian fit as $33.3\%\sqrt{E}$.

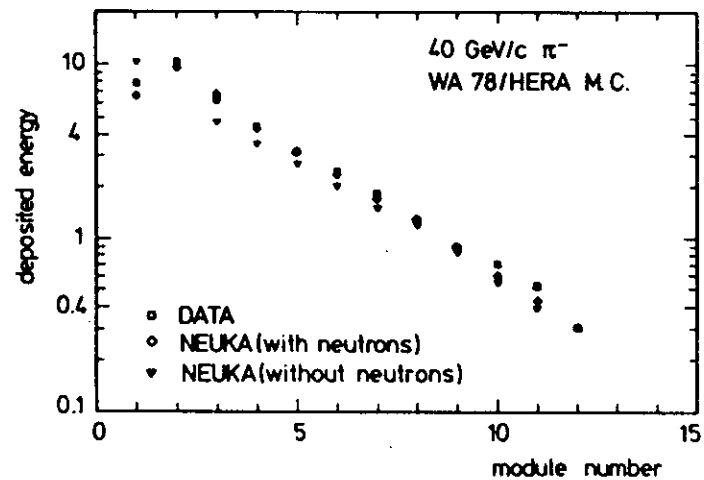
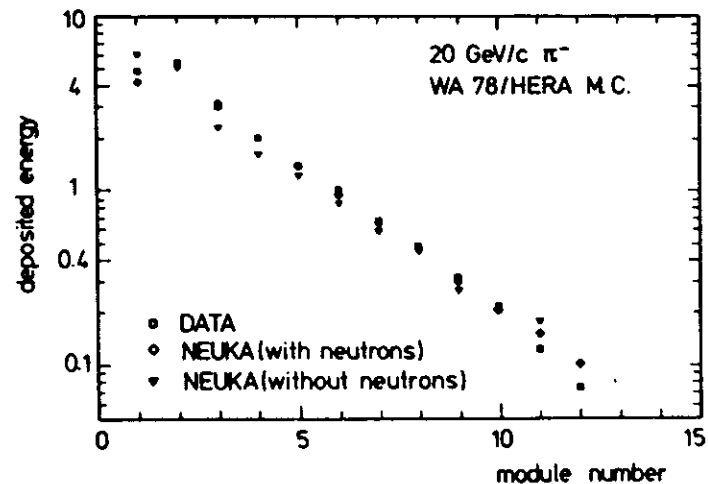


Fig. 13. Comparison of longitudinal shower development profiles observed in test WA78 and NEUKA predictions. The longitudinal axis is defined in the module number units (a module thickness was around 0.43λ). The deposited energy is given in GeV. The data and MC calculation are normalised to the beam energy.

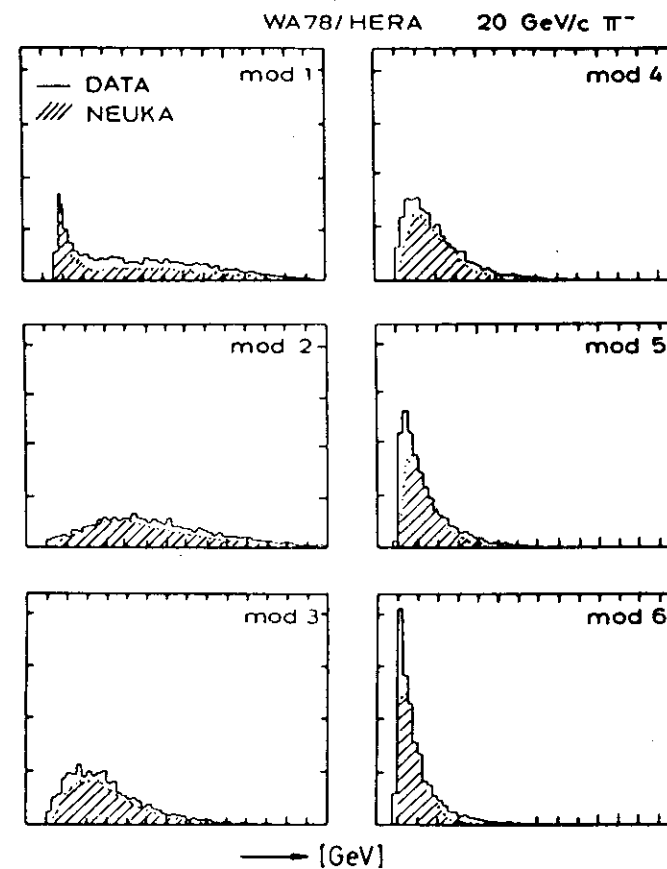


Fig. 14. Comparison of the observed energy distributions in the first six modules of the test WA78 with NEUKA predictions. (a module thickness was around 0.43λ). The MC calculation is only approximately normalised to the beam energy.

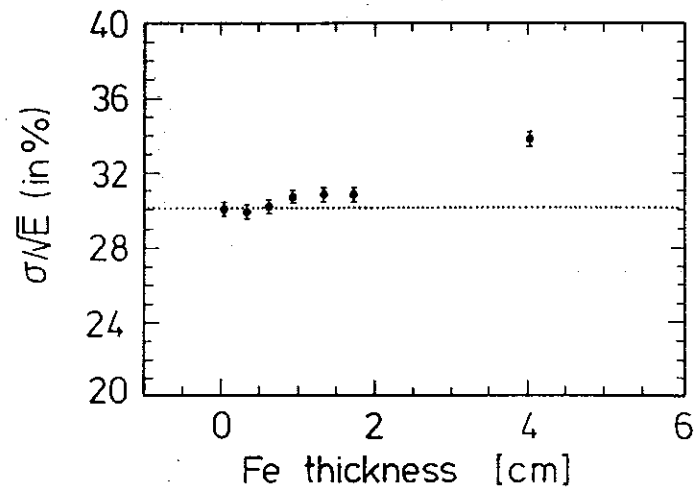


Fig 15. Resolution for the infinite calorimeter as a function of the iron plate thickness introduced into the structure after $1 \lambda_{int}$

infinite calorimeter as a function of the iron plate thickness. ZEUS collaboration measured recently the effects of iron plate inside the Test 60 calorimeter and obtained results similar to our computation.

Acknowledgements

We would like to thank many of our colleagues from the ZEUS collaboration and in particular H. Brueckmann, B. Anders, R. Klanner and G. Wolf for many useful discussions. T. Tsurugai helped us considerably in preparing some of the results presented in this talk. We are also indebted to B. Foster and C. Youngman for correcting our sometimes slightly grotesque English.

REFERENCES

- Ref. 1. P.A. Arnio, A. Fasso, H-J. Moehring, J. Ranft G. R. Stevenson, FLUKA86 User's Guide, CERN TIS-RP/168
- Ref. 2. J. Ranft, J.T. Routti, Particle Accelerators 4, 101, (1972)
- Ref. 3. C. Leroy, Y. Sirois, R. Wigmans, NIM A252, 4, (1986)
- Ref. 4. H. Brueckmann, B. Anders, U. Behrens, P. Cloth, D. Filges, On the Theoretical Understanding and Calculation of Sampling Calorimeters, DESY 87-064
- Ref. 5. R. Wigmans, On the Energy Resolution of Uranium and Other Hadron Calorimeters, CERN/EF 86-18 (1986)
- Ref. 6. V.M. Gorbachev, Y.S. Zamyatin, A.A. Lbov, Nuclear Interactions in Heavy Elements, Pergamon Press (1980)
- Ref. 7. E. Sheldon et al., Journal of Phys. G, Nucl. Phys. 12, 443 (1986)
- Ref. 8. R.D. Evans, The Atomic Nucleus, Mc Graw-Hill(1955)
- Ref. 9. M. Caner et al., Nuclear Science and Engineering 59, 395 (1976)
- Ref. 10. J.W. Meadows, Phys. Rev. 157, 1076 (1967)
- Ref. 11. G. Bathow et al., Nuclear Physics, B20, 592 (1970)